Mon. Not. R. Astron. Soc. **000**, 1–?? (2002) Printed 2 February 2008 (MN LaTeX style file v2.2)

Theoretical Light Curves of Type II-P SNe and Applications to Cosmology

A. Chieffi,[1,4], I. Domínguez,[2], P. Höflich,[3], M. Limongi,[4], O. Straniero,[5]
[1] *Istituto di Astrofisica Spaziale e Fisica Cosmica (CNR), Via Fosso del Cavaliere, I-00133 Rome, Italy, achieffi@rm.iasf.cnr.it*
[2] *Dept. Física Teórica y del Cosmos, Universidad de Granada, E-18071 Granada, Spain, inma@ugr.es*
[3] *Dept. of Astronomy, University of Texas, Austin, TX78681, USA, pah@astro.as.utexas.edu*
[4] *INAF-Osservatorio Astronomico di Roma, Via Frascati 33, I-00040 Monteporzio Catone, Italy, marco@mporzio.astro.it*
[5] *INAF-Osservatorio Astronomico di Teramo, I-64100 Teramo, Italy, straniero@te.astro.it*

Released 2002 Xxxxx XX

ABSTRACT

Based on an extensive grid of stellar models between 13 and 25 $M_\odot$ and a wide range of metallicities, we have studied the light curves of core collapse supernovae, their application to cosmology and evolutionary effects with redshift. The direct link between the hydro and radiation transport allows to calculate monochromatic light curves.

With decreasing metallicity Z and increasing mass, progenitors tend to explode as compact Blue Supergiants (BSG) and produce sub-luminous supernovae that are about 1.5^m dimmer compared to *normal* SNe II with Red Supergiant (RSG) progenitors. Progenitors with small masses tend to explode as RSGs even at low Z. The consequences are obvious for probing the chemical evolution, namely, a strong bias when using the statistics of core collapse supernovae to probe the history of star formation.

Our study is limited in scope with respect to the explosion energies and the production of radioactive Ni. Within the class of *extreme SNe II-P* supernovae, the light curves are rather insensitive with respect to the progenitor mass and explosion energy compared to analytic models which are based on parameterized stellar structures. We expect a wider range of brightness due to variations in ^{56}Ni because radioactive energy is a main source of luminosity. However, the overall insensitivity of LCs may allow their use as quasi-standard candles for distance determination.

Key words: stars: evolution - supernovae: Type II - cosmology: distance scale.

1 INTRODUCTION

Core collapse supernovae, are thought to be the final results of stellar evolution for stars with main sequence masses $\gtrsim$ 10 $M_\odot$ with evolutionary time scales short compared to the age of the universe even at high z (Tammann, 1982; Maza & Van den Bergh, 1976; Woosley & Weaver 1986). These objects will occur soon after the initial star formation period and, therefore, can be used to probe the structure of the universe at high *z*. These very distant supernovae are all expected to be some variety of core collapse supernovae. E.g. at $z \sim 5$ to 10, galaxies are expected to be small and dim and core collapse supernovae may be the brightest objects in the Universe (Miralda-Escudé & Rees 1997).

The light curves and spectra depend sensitively on the initial stellar mass, metallicity, mass loss and explosion energy. They show a wide range of brightness, up to 6 magnitudes, and properties of their light curves (Filippenko, 2000; Patat et al. 1993 & 1994; Young & Branch, 1989) that prevents their use as standard-candles. However, our knowledge of the event is improving and it may be possible to derive the absolute magnitude in a similar way as Type Ia if appropriate empirical correlations can be identified.

There is a general agreement that the explosion of a massive star is caused by the collapse of its central parts into a neutron star or a black hole. The mechanism of the energy deposition into the envelope is still debated. The process likely involves the bounce and the formation of the prompt shock (e.g. Van Riper 1978, Hillebrandt 1982), radiation of the energy in the form of neutrinos (e.g. Bowers & Wilson 1982), the interaction of the neutrinos with the material of the envelope and various types of convective motions (e.g. Herant et al. 1994, Burrows et al. 1995, Müller & Janka 1997, Janka & Müller 1996), rotation (e.g. LeBlanc & Wilson 1970, Saenz & Shapiro 1981, Mönchmeyer et al. 1991), and magnetic fields (e.g. LeBlanc & Wilson 1970, Bisnovati-Kogan 1971).

The analysis of core collapse supernovae and their use for cosmology is further complicated due to the mounting evidence that the explosions of massive stars (core collapse SN) are highly aspherical and, consequently, the brightness depends on their orientation to the observer (e.g. Höflich 1991b). (1) The spectra (e.g. SN87A, SN93J, SN94I, SN99em) are significantly polarized indicating asymmetric envelopes (Méndez et al. 1988; Höflich 1991b; Jeffrey 1991; Wang et al. 1996; Wang, Wheeler & Höflich 1999). The degree of polarization tends to vary inversely with the mass of the hydrogen envelope, being maximum for SNe Ib/c events with no hydrogen (Wang et al. 2000, Leonard et al. 2002). For supernovae, with a good time and wavelength coverage, the orientation of the polarization vector tends to stay constant both in time and in the wavelength. This suggests that there is a global symmetry axis in the ejecta (Leonard et al. 2001). (2) Observations of SN 1987A showed that radioactive material was brought to the hydrogen rich layers of the ejecta very quickly during the explosion (Tueller et al. 1991). (3) The remnant of the Cas A supernova shows rapidly moving oxygen-rich matter outside the nominal boundary of the remnant and evidence for two oppositely directed jets of high-velocity material (Fesen & Gunderson 1997). (4) Recent X-ray observations with the CHANDRA satellite have shown an unusual distribution of iron and silicon group elements with large scale asymmetry in Cas A (Huges et al. 2000). (5) After the explosion, neutron stars are observed with high velocities up to 1000 km/s (Strom et al. 1995).

Due to the difficulty of modeling core collapse from first principles, a very different line of attack on the explosion problem has been used extensively and proved to be successful in understanding the supernova problem, SN1987A in particular (Arnett et al. 1990, Hillebrand & Höflich 1991). The difference of characteristic time scales of the core (a second or less) and the envelope (hours to days) allows one to divide the explosion problem into two largely independent parts - the core collapse and the ejection of the envelope. By assuming the characteristics of the energy deposition into the envelope during the core collapse, the response of the envelope can be calculated. Thus one can study the observational consequences of the explosion and deduce characteristics of the core collapse and the progenitor structure. This approach has been extensively applied in the framework of the 1D spherically symmetric formulation. The major factors influencing the outcome have been found to be the explosion energy and the progenitor structure. Recently, the same approach has been applied in multi-dimensions to investigate the effects of asymmetric explosions (e.g. Höflich et al. 2001). First results show that both asymmetric density structures and excitations are keys for our understanding of the global asymmetries in core collapse supernovae.

Despite these problems, methods have been developed to use these objects for distance determinations, namely, SNe II that have retained their H-rich envelope. SNe II represent an important complement to SNe Ia as a technique to measure cosmological distances. In principle, the distance to each individual SNe II can be measured by the *Baade-Wesselink* or *Expanding Photosphere* method in which the ratio of the observed apparent flux to the absolute flux gives the solid angle, and the velocity and elapsed time give the radius (e.g. Shaviv et al. 1985, Höflich et al. 1986, Branch et al. 1988, Höflich 1988, 1991, Schmidt et al. 1994, Leonard et al. 2002).

Recently a sub-group of SNe II, SNe II-P, has been proposed as good quasi-standard candles (Höflich et al. 2000, Hamuy and Pinto 2002), decreasing the scatter in the Hubble diagram. The plateau in the SN II-P light curve, that is caused by the recombination of H, is indicative of a massive H envelope. Thanks to the plateau the identification does not require any spectra and it is not necessary to follow the event to dimmer phases. We identify a subclass among SNe II-P, *extreme* SNe II-P, characterized by a *long* plateau, with a duration exceeding 50-60 days. Notice that the characteristic time of the plateau observed by the telescopes is increased by a factor $(1+z)$ (ie. at z=3, the *bright* observed plateau lasts several months).

Although, their statistic is still very incomplete, *extreme* SNe II-P are probably as frequent as SNe Ia in the nearby universe (Cappellaro et al. 1999). In the years 1998 and 1999 around a 10% of all SNe II could be classified as *extreme* SN II-P. However, this is expected to change at *intermediate* redshifts ($z \approx$ 3-5) when the star formation rate was higher (Kravtso & Yepes, 2000). At the other hand, SNe II maybe the only SNe at $z \geqslant$3-5. Moreover, at $z \geqslant$10, they may be the only luminous objects, out-shining the host proto-galaxy by a factor of 100 during more than 2 years (Marri & Ferrara 1998). Cold Dark Matter (CDM) models, taken into account gravitational magnification, predict in 100 fields of the Next Generation Space Telescope around 850 and 3500 SNII/year (for Standard and Lambda CDM models, respectively) up to a redshift of z=15 (Marri, Ferrara & Pozzetti, 2000).

One key problem to be addressed will be to determine whether these events will look like local supernovae that explode as red supergiants, or whether, because of their low metallicity they will all resemble SN 1987A that exploded as a blue supergiant (see also Brunish & Truran 1982). Prediction of the properties of these early supernovae now will set the stage for the work of upcoming observational facilities, like NGST, SNAP and others.

Very few studies of light curves of SNe II-P have been published up to now. Litvinova & Nadëzhin (1983,1985) presented a grid for a range of envelope masses between 1 and 16 $M_\odot$ that, some 20 years later, still presents the most comprehensive study. The models assumed spherical symmetry and parameterized density profiles, and 4 basic free parameters: input energy, the amount of radioactive Ni and the envelope mass and initial radius. The result of these calculations were theoretical bolometric lightcurves which were then converted into V-band lightcurves assuming a black body energy distribution. Some of these restrictions have been overcome in the analysis of Eastman et al. (1994) but this study has been restricted to a star with 15 $M_\odot$. Both studies cannot answer the key problems mentioned above. In this paper, we link the pre-SN evolutionary models to SN models. One big advantage is that the initial radius of the SN models is no longer an adjustable parameter but a result of the physical model and a function of the stellar mass. The other progress is that the hydro models are linked to a radiative transport code, so the broad-band lightcurves are much more accurately computed. A third progress provided by this paper is the effect of metallicity in the resulting lightcurves.

Following the successful approach to assume the char-

acteristics of the energy deposition at the inner regions of the exploding star, we present explosion models and theoretical light curves for a wide range of stellar masses and metallicities. The goal of this study is to explore the sensitivity of different characteristics of the SN II-P light curves on the underlying progenitor properties (initial mass and metallicity) and the kinetic energy based on detailed stellar evolution and LC calculations. Effects due to stellar rotation and mass loss during the evolution of the progenitor are not included. Moreover, these calculations do not address the mechanism of energy deposition, production of radioactive Ni, chemical mixing and departures from sphericity. One of our main results is the identification of *extreme* SN II-P, as potential candidates to be use in cosmology. Note that we do not intend to provide a complete grid of models to be compared with specific observations. In this work, we present a study focused on core collapse supernovae to answer the following questions: How do the light curves of core collapse supernovae depend on the metallicity that is expected to decrease with redshift? Can we identify a subclass among the core collapse supernovae that may be used as quasi-standard candles, and what accuracy do we expect? Can this subclass be identified purely by their light curves, without a follow-up that requires to *go* much fainter than maximum light?

The outline of the paper is as follows: in Section 2 the numerical methods used for the evolution, explosion and light curves computations are described, in Section 3 the influence of the progenitor properties and explosion parameters on the light curves are analyzed, and finally, in Section 4, we highlights the main conclusions and short-comes of our study.

2 NUMERICAL METHODS

2.1 Stellar Evolution

All the pre-supernova models adopted in this paper have been computed by means of the evolutionary code FRANEC, rel 4.2 (for details see Chieffi & Straniero 1989, Chieffi, Limongi & Straniero 1998, Limongi, Straniero & Chieffi 2000, Straniero, Chieffi and Limongi 1997 and Chieffi & Limongi 2002). The FRANEC is an hydrostatic evolutionary code in which both the set of equations describing the physical structure of the star (by assuming spherical symmetry) and the chemical evolution of the matter, due to the nuclear reactions, are fully coupled and integrated simultaneously by means of a classical Newton -Raphson method. The nuclear network includes 41 isotopes for the H burning, 88 isotopes for the He burning and 179 isotopes for the more advanced phases. Nuclear reaction rates are taken from the Thielemann's database (private communication). For the $^{12}C(\alpha,\gamma)^{16}O$ reaction we adopt the value from Caughlan et al. (1985) which is close to the upper limit compatible with the presently available measurements for this rate. The weak interaction rates as a function of the temperature and density are derived from Fuller, Fowler & Newman (1980, 1982 and 1985).

The extension of the convective regions are fixed by means of the Schwarzschild criterion and no mechanical overshoot is allowed. Induced overshooting and semiconvection during core He burning are taken into account (Castellani et al. 1985). In the convective layers the temperature gradient is evaluated by means of the mixing length theory as described by Cox & Giuli (1968). A time dependent mixing scheme is used which is similar to the one firstly introduced by Sparks & Endal (1980). We have also developed a specific algorithm which can handle the evolution of those isotopes whose nuclear burning lifetime becomes comparable or lower than the mixing timescale (see Chieffi, Limongi & Straniero 1998).

Electron screenings are taken from Graboske et al. (1973) for the weak, intermediate and intermediate-strong regime, and from Itoh, Totsuji & Ichimaru (1977) and Itoh et al. (1979) for the strong regime. The equation of state (EOS) is the one described by Straniero (1988) and updated by Straniero, Chieffi and Limongi (1997). It includes Coulomb corrections, quantum-relativistic effects on the electron component and electron-positron pairs production. Radiative opacity coefficients are derived from Kurucz (1991), Alexander & Fergusson (1994), Iglesias, Rogers & Wilson (1992) (OPAL) and from the Los Alamos Opacity Library (LAOL) (Huebner et al. 1977). A scaled solar mixture (Grevesse 1991) is adopted. Opacity coefficients due to the thermal conductivity are derived from Itoh et al. (1983). Energy loss due to photo, pair and plasma neutrinos are taken into account following Munakata, Kohyama & Itoh (1985), Munakata, Kohyama & Itoh (1986). Bremsstrahlung neutrinos are obtained following Dicus et al. (1976) as corrected by Richardson et al. (1982). Energy losses due to the recombination processes are included by using the prescriptions of Beaudet, Petrosian & Salpeter (1967).

In this work, all the models are evolved at constant mass and no rotation has been taken into account. The effects of rapid rotation in the evolution of massive stars have been recently studied in 1D by Heger, Langer and Woosley (2000) and Meynet and Maeder (2000,2003). As discussed in the introduction, the explosion mechanism itself could be based on rotation but the effect on the hydrodynamics of the H-rich envelope are expected to be small. However, anisotropies in the Ni distribution and, thus, the ionization may cause anisotropic luminosities of the order of of 10 % (Höflich 1991, Höflich et al. 2001).

2.2 Explosion and Light Curve Models

The explosions are calculated using our one-dimensional radiation-hydro code, including nuclear networks (Höflich & Khokhlov 1996 and references therein). This code solves the hydrodynamical equations explicitly by the piecewise parabolic method (Collela & Woodward 1984) and includes the solution of the frequency averaged radiation transport implicitly via momentum equations, expansion opacities (see below), and detailed equation of state. For high densities and temperatures ($\geqslant 1 g/cm^3$, $\geqslant 10^7$ K), relativistic effects are taken into account and full ionization is assumed. For lower densities and temperatures, ionization processes are included under the assumption of local thermodynamical equilibrium but relativistic effects are neglected.

The explosion is triggered artificially by depositing energy at a mass location near the edge of the iron core. After the initial phase of the explosion, i.e. shortly before the shock front reaches the stellar surface, the nuclear reac-

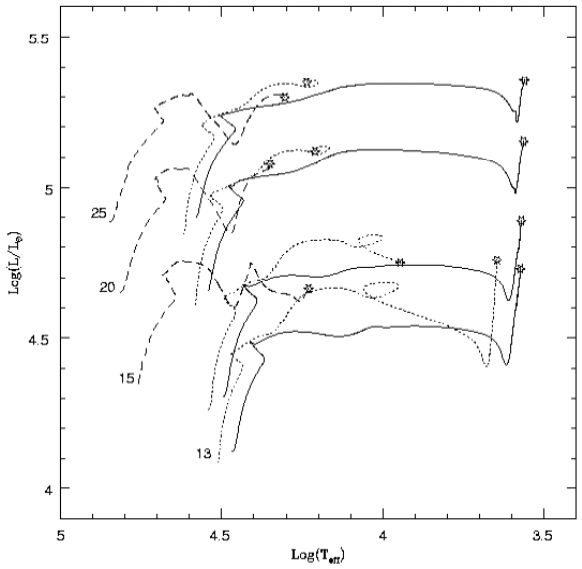

Figure 1. Presupernova evolutionary path in the HR diagram of models 13, 15, 20 and 25 $M_\odot$ having metallicities Z=0.02 (solid), 0.001 (dotted), and 0 (dashed).

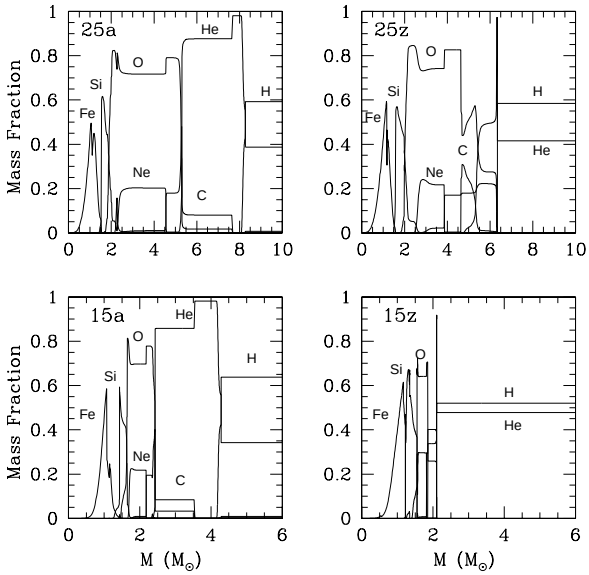

Figure 2. Chemical composition of selected models at the onset of core collapse.

tions are switched off and γ ray transport is included via a Monte Carlo scheme. Both monochromatic and bolometric light curves are calculated using a scheme recently developed, tested and widely applied to SNe Ia (Höflich et al. 1998, and references therein). In order to allow for a more consistent treatment of scattering, we solve both the (two lowest) time-dependent, frequency averaged radiation momentum equations for the radiation energy and the radiation flux, and a total energy equation. At each time step, we then use $T(r)$ to determine the Eddington factors and mean opacities by solving the frequency-dependent radiation transport equation in the comoving frame and integrate to obtain the frequency-averaged quantities. The averaged opacities are calculated under the assumption of local thermodynamical equilibrium. Both the monochromatic and mean opacities are calculated using the Sobolev approximation. The scattering, photon redistribution and thermalization terms used in the light curve opacity calculation are calibrated with NLTE calculations using the formalism of the equivalent-two-level approach (Höflich 1995). About one thousand frequencies and between 550 to 700 depth points are used.

3 RESULTS

3.1 Stellar Models

The evolution of selected models in the mass range from 13 $M_\odot$ to 25 $M_\odot$ and metallicities between Z=0 and Z=0.02 have been computed from the pre-main sequence to the onset of core collapse without mass loss (see Fig. 1 and Table 1). For low metallicities Z, models explode as compact BSG ($R_\star \leqslant 100 R_\odot$) rather than as extended RSG ($500 R_\odot \leqslant R_\star \leqslant 1500 R_\odot$). The metallicity plays a major role in determining the radius of the star because it affects the opacity that determines the super-adiabatic gradient. The larger the opacity, the larger the super-adiabatic gradient and hence the larger the radius of the star. This explains why for low metallicities, stars explode as blue supergiants. In general, the stellar radius depends on the opacity of the envelope; the lower is the metallicity the lower is the opacity of the envelope and, as a consequence, the more compact is the structure. We find that all the zero metallicity models end up as a BSG while all the solar metallicity ones end up as a RSG. At intermediate Z, there is the general trend that the more massive stars end up as BSG while the less massive ones end up as RSG. The limiting mass depends on Z. However, the critical metallicity beyond which a star ends as RSG instead of a BSG depends sensitively on many details among which the treatment of convection, the opacities, rotation and mass loss.

In Table 1 we report selected properties of the presupernova evolutions, namely: the identification name of the models, Mnnx, nn is the mass and x refers to metallicity, "a" is for solar (Z=0.02), "b" for Z=0.001 and "z" for Z=0 (column 1); the mass in solar units (column 2); the final radius in solar radii (column 3); the metallicity (column 4); BSG vs. RSG (column 5); the hydrogen burning lifetime in years (column 6); the helium burning lifetime in years (column 7); the residual lifetime following the central He exhaustion up to the iron core collapse (column 8); the final surface mass fraction of H (column 9) and He (column 10).

Figure 2 shows the chemical composition at the onset of the iron core collapse, for some of the computed stellar models. Figure 3 illustrates the influence of both metallicity (upper panel) and initial mass (lower panel) on the density profiles. As it is well known, the smaller the total mass the less compact is the star. By comparing Figure 2 and 3 it appears that the last (most external) sudden drop in the density profiles corresponds to the transition to the H-rich envelope. From this point to the surface the density-mass relation is essentially independent on the initial mass, while, on the contrary, it is significantly affected by a metallicity variation. As it will be discussed in more details in the fol-

Table 1. Selected quantities of the some of the stellar models

Model	Mass	R_{fin} ($R_\odot$)	Z	BSG vs. RSG	τ_H(yr)	τ_{He}(yr)	τ_{adv}(yr)	H_{sup}	He_{sup}
m13a	13	$5.52 \cdot 10^2$	$2 \cdot 10^{-2}$	RSG	$1.26 \cdot 10^7$	$1.92 \cdot 10^6$	$6.57 \cdot 10^4$	0.649	0.331
m15a	15	$6.71 \cdot 10^2$	$2 \cdot 10^{-2}$	RSG	$1.08 \cdot 10^7$	$1.45 \cdot 10^6$	$3.87 \cdot 10^4$	0.638	0.342
m20a	20	$9.40 \cdot 10^2$	$2 \cdot 10^{-2}$	RSG	$7.50 \cdot 10^6$	$9.53 \cdot 10^5$	$2.29 \cdot 10^4$	0.609	0.371
m25a	25	$1.19 \cdot 10^3$	$2 \cdot 10^{-2}$	RSG	$5.97 \cdot 10^6$	$6.99 \cdot 10^5$	$1.67 \cdot 10^4$	0.593	0.387
m13b	13	$4.08 \cdot 10^2$	$1 \cdot 10^{-3}$	RSG	$1.47 \cdot 10^7$	$1.80 \cdot 10^6$	$6.03 \cdot 10^5$	0.708	0.291
m15b	15	$1.01 \cdot 10^2$	$1 \cdot 10^{-3}$	BSG	$1.22 \cdot 10^7$	$1.41 \cdot 10^6$	$4.17 \cdot 10^5$	0.769	0.230
m20b	20	$4.60 \cdot 10^1$	$1 \cdot 10^{-3}$	BSG	$8.84 \cdot 10^6$	$8.71 \cdot 10^5$	$2.47 \cdot 10^4$	0.769	0.230
m25b	25	$5.26 \cdot 10^1$	$1 \cdot 10^{-3}$	BSG	$7.09 \cdot 10^6$	$6.69 \cdot 10^5$	$1.80 \cdot 10^4$	0.769	0.230
m15z	15	$2.48 \cdot 10^1$	0.0	BSG	$1.05 \cdot 10^7$	$9.27 \cdot 10^5$	$5.44 \cdot 10^4$	0.770	0.230
m20z	20	$2.31 \cdot 10^1$	0.0	BSG	$7.74 \cdot 10^6$	$5.76 \cdot 10^5$	$2.39 \cdot 10^4$	0.770	0.230
m25z	25	$3.67 \cdot 10^1$	0.0	BSG	$6.72 \cdot 10^6$	$4.96 \cdot 10^5$	$1.59 \cdot 10^4$	0.770	0.230

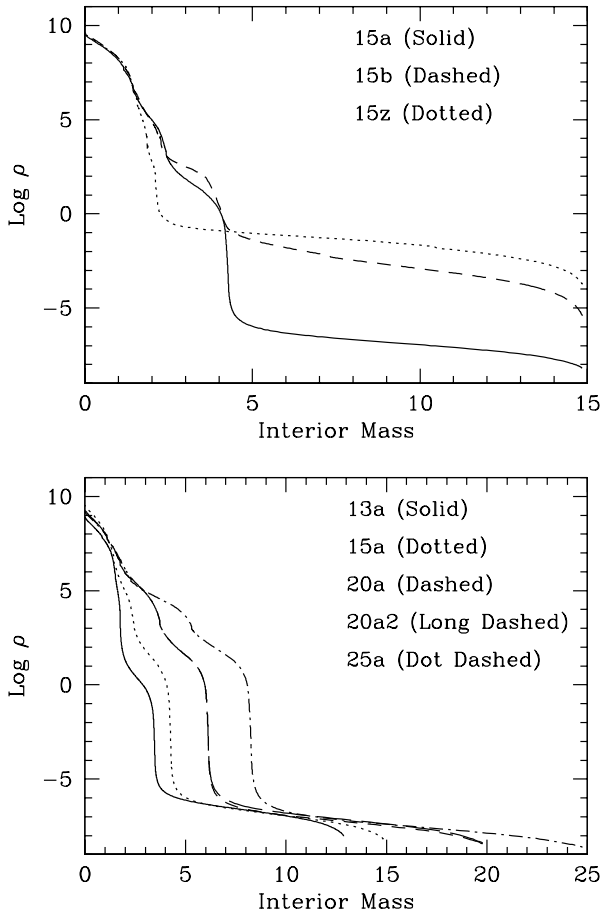

Figure 3. Stellar density structure as a function of mass for different metallicities (upper panel) and initial masses (lower panel). Note the similarity between the density profiles of the two BSGs, 15b and 15z (upper panel). To test the convergence of the resolution in our models, we have increased the number of depth points by a factor of 10 in model 20a, the resulting structure, 20a2 (see lower panel), is almost identical.

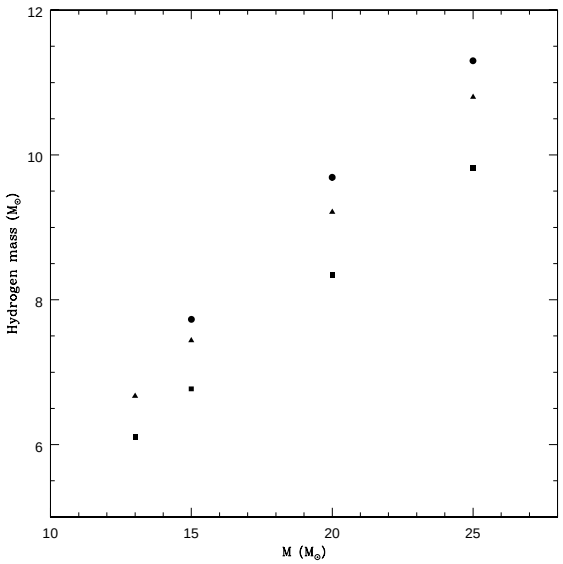

Figure 4. Final hydrogen mass as a function of total mass for different metallicities: Z=0.02 (squares), Z=0.001 (triangles) and Z=0 (circles)

lowing sections, such a correlation between the density of the H rich envelope with the mass and the metallicity of the stellar progenitor has a significant influence on the features of the various light curves, in particular on the plateau phase (namely the first 100-150 days). In fact during this phase, the H recombination front, that provides the nearly constant luminosity, moves inward (in mass) through the whole envelope.

Another important quantity that characterizes the light curve is the total amount of H present in the envelope. In principle, it depends on the original chemical composition of the star, on the initial mass, on the mass loss rate and on the efficiency of the various dredge up episodes occurring during the progenitor life. In Figure 4 we have reported the final H mass as a function of the total mass for the 3 different metallicities. Note that the final H mass linearly increases as the stellar mass increases and the metallicity decreases. We find that the following relation nicely reproduces the results of our stellar evolution calculations:

$M_H(M_\odot)$=2.58+0.338 $\cdot M(M_\odot)$- 50.3 $\cdot Z$

where M_H, M and Z are the total H mass, the total stellar mass and the metallicity, respectively. Since our models were obtained without mass loss, this relation provides an upper limit for the final amount of H.

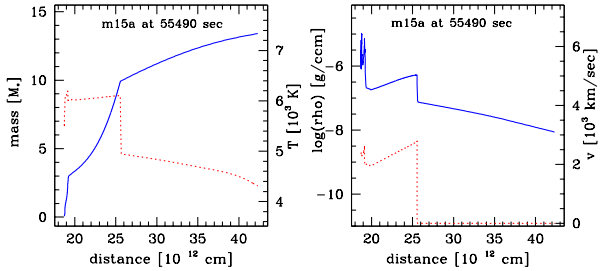

Figure 5. Structure of the 15 $M_\odot$, Z=0.02 model with a final kinetic energy of 10^{51} erg (model m15a) 15.4 hours after the explosion. Integrated mass M(r) (solid) and T(r) (dotted) are given in the left plot, ρ(r) (solid) and v(r) (dotted) are given in the right plot.

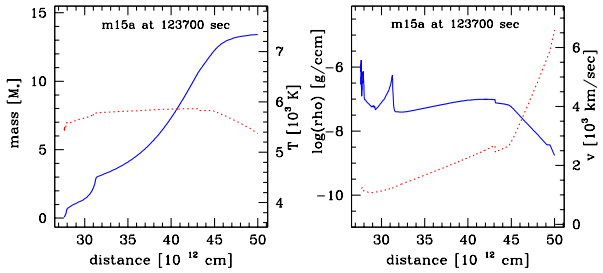

Figure 6. Same as Fig. 5 but 34.3 hours after the explosion, just after shock breakout.

3.2 Explosion Models

Based on the evolutionary models previously described, we have explored the sensitivity of different characteristics of the light curve on progenitor properties (mass and metallicity) and explosion energy. The explosion is triggered by depositing a given amount of energy at a mass coordinate close to the edge of the iron core of the presupernova model, i.e. at about 1.4 $M_\odot$ that, in turn, corresponds to about 1000 km in all the models. The injected energy is properly adjusted in order to provide the desired final kinetic energy. In all models except one, the final kinetic energy is 10^{51} erg, the exception is model m15a; for this model we consider also the case with a final kinetic energy of $2{\cdot}10^{51}$ erg (hereafter model m15a2). For test calculations, the explosion energy has been deposited both as thermal or kinetic energy but little difference has been found in the explosion models.

In general, at a given time after the explosion has been

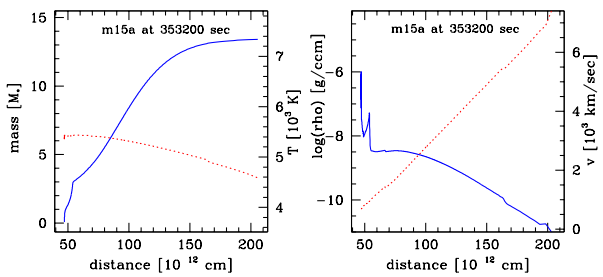

Figure 7. Same as Fig. 5 but 98 hours after the explosion when the expansion of the envelope is almost homologous.

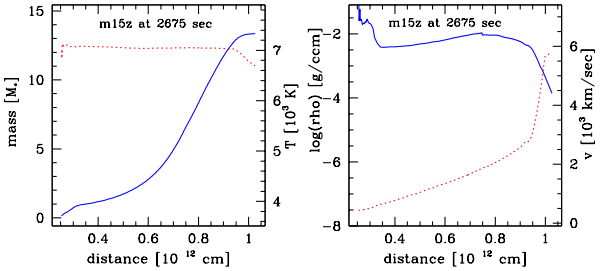

Figure 8. Same as Fig. 5 but for the model m15z, Z=0.0 at about 44 minute after the explosion just after shock breakout.

triggered, the velocity of the more internal zones of the exploding envelope drops down to the escape velocity. As a consequence, these zone will eventually and naturally fall back onto the compact remnant. The final mass location between the ejecta and the remnant is defined as the mass cut. The fallback of material on the central neutron star remained smaller than 10^{-2} $M_\odot$ except in the more massive models. A significant fallback of 0.1 and 0.47 $M_\odot$ was obtained for m20a and m25a, respectively. We note that the amount of fallback depends sensitively on the explosion energy. In test calculations for m25a with twice the explosion energy, the fallback was reduced by about a factor of 5. In all cases, but for 25 $M_\odot$, more than a tenth of a solar mass of ^{56}Ni would be ejected which is in excess of the typical amount obtained from the observed luminosity of the light curve tail. For this reason we introduced an *artificial* mass cut (more external than the actual mass cut) in the explosion models at about one day after the explosion to limit the ^{56}Ni production accordingly. In this work we adopt the typical value of 0.07 $M_\odot$ (e.g. SN1987A) for the ^{56}Ni mass, although some SN II-P are known to have more than a tenth (e.g. SN1992am, 0.3 $M_\odot$, Schmidt et al. 1994; 1986I, 1991G, 1992H, Hamuy 2002).

A further restriction of our models is related to the discretization in mass which is of the order of 10^{-3} $M_\odot$. A proper resolution of the photosphere during the first few days of the explosion requires a discretization of about 10^{-5} $M_\odot$ (e.g. Müller & Höflich, 1991). Consequently, details of the shock breakout are beyond the scope of this study because the photosphere is not well resolved at the early phases.

In Table 2, the basic parameters and some of the derived quantities are given for the explosion models and light curves. Let's concentrate here in the first 4 columns: identification of the model, as in Table 1 (column 1); final kinetic energy after the explosion (column 2); time of the shock breakout in seconds (column 3) and the corresponding temperature T_{shock} at the photosphere (column 4).

In Figs. 5 to 7, a typical evolution of the exploding star is given at the example of model m15a. Initially, the shock front propagates outward and deposits energy in form of thermal energy. Weaker, reversed fronts are created at the chemical boundaries. For m15a, after about 1.5 days, the shock front reaches the outer stellar layers. The shock front is accelerated because of the steep density profiles at the surface layers of the star (Fig. 3), and produces a rapidly expanding outward layer (see Figure 6, right panel). During the following time, most of the thermal energy is used

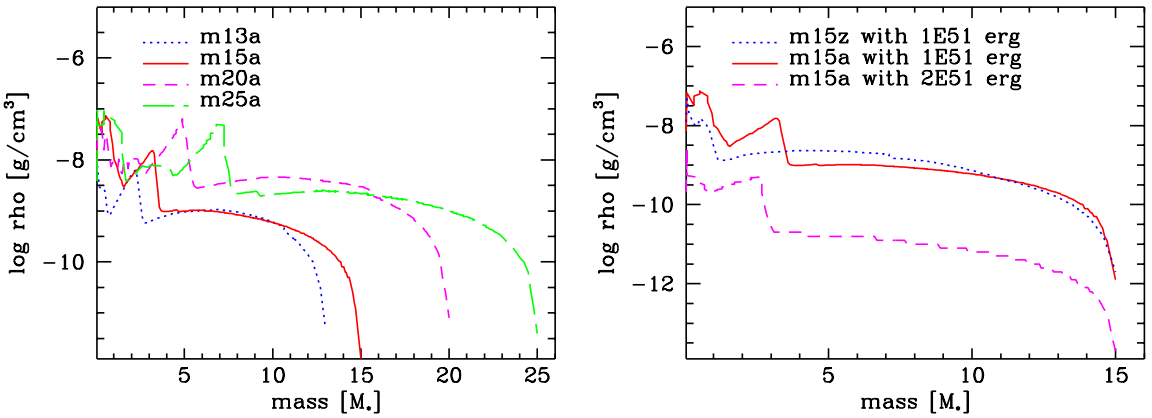

Figure 9. Density profiles at day 5 for models with various masses (left panel), metallicities end kinetic energies (right panel).

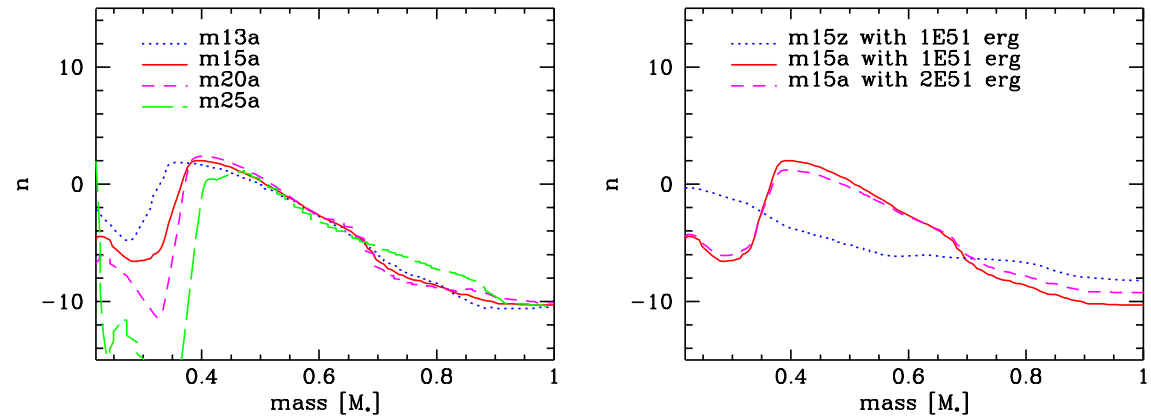

Figure 10. Same as Fig. 9 but for the density gradients n ($\rho \propto r^{-n}$). In the x axis the interior mass is normalized to 10 $M_\odot$.

to overcome its potential, do expansion work, and accelerate the expanding envelope. After about 3-4 sound crossing times of the progenitor, the expansion of the envelope is almost homologous, i.e. $v \propto r$, ending the phase dominated by hydrodynamics (see Fig. 7, right panel). Subsequent energy release by radioactive decays causes only minor modifications of the density profile. We note that, in reality, some interaction with the surrounding medium may become important.

All models show a behavior very similar to our example with some quantitative differences. For example, in case of the explosion of a compact, blue supergiant, the shock front reaches the surface already after about one hour and the breakout temperatures are significantly larger, and subsequently, adiabatic cooling is increased drastically (see Table 2 and Fig. 8).

The times till the shock breakout t_{shock} (Table 2) are consistent with the analytical approximation by Shigeyama et al. (1988) who found that t_{shock} scales with the stellar radius, and with the square of the mass and explosion energy. In our models, typical times are of the order of days for RSGs (1 to 3 days) and hours for BSGs (1 to 3 hours).

It is worth noting that the peak temperatures for red supergiants are rather low whereas blue supergiants can reach peak temperatures in excess of a million degrees (see Table 2). The possible consequences for the contribution of the production of high energy photons at large redshifts shall be noted and its implications for environment will be discussed in the Conclusions.

Density structures and density gradients are given in Figures 9 and 10, respectively. As can be expected from the discussion of the stellar profiles (Fig. 3), the final density structures are rather similar for the red supergiants. For the blue supergiants, the density profiles are significant steeper in the inner layers of the hydrogen rich envelope which, as we will see, has strong effects on the light curve.

3.3 Light Curves

In this section, we will discuss the phase when the properties of the envelope are mainly determined by free expansion and radiative processes and the energy release is governed by stored energy, thermal energy, recombination processes and radioactive decay.

In general, an early maximum is seen which is produced by the release of the stored thermal energy, followed by a plateau phase due to the recombination of H and, finally, a

Table 2. Explosion models and Light Curve properties.

Model	E_{kin} [10^{50} erg]	t_{shock} [s]	log(T_{shock})	V_{max}	$\delta t_{plateau}$ [days]	δm_{bump} [mag]
m13a	10	$1.33{\cdot}10^5$	5.5	-17.49	45	0.15
m15a	10	$1.21{\cdot}10^5$	5.4	-17.47	66	0.22
m20a	10	$2.10{\cdot}10^5$	5.3	-17.44	73	0.29
m25a	10	$3.10{\cdot}10^5$	5.2	-17.42	78	0.39
m15a2	20	$8.47{\cdot}10^4$	5.6	-17.74	79	0.26
m15b	10	$9.23{\cdot}10^3$	5.9	-16.43	dna	dna
m15z	10	$2.62{\cdot}10^3$	6.7	-16.20	dna	dna

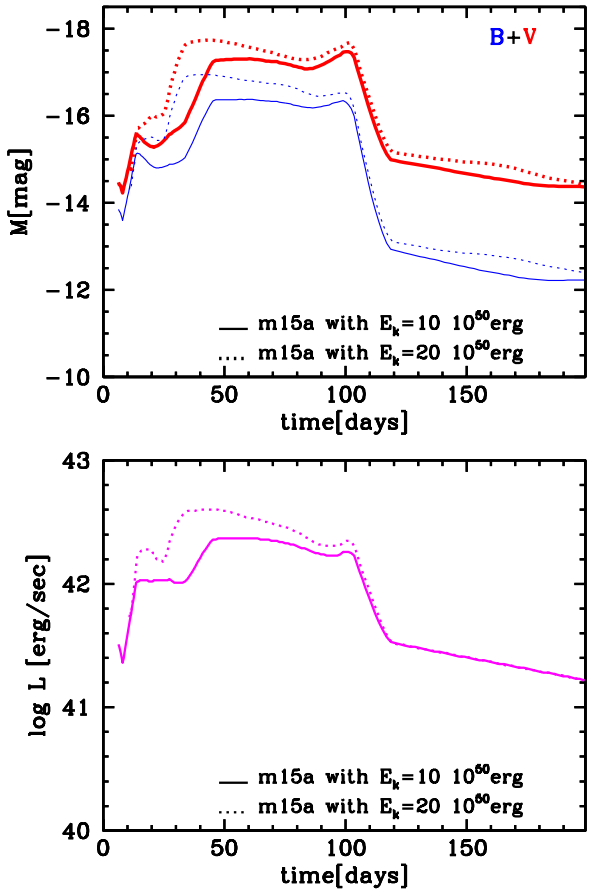

Figure 11. Light curves for the 15 $M_\odot$, Z=0.02 model with two final kinetic energies, $10^{51} erg$ and $2{\cdot}10^{51} erg$, models m15a and m15a2 in Table 2, respectively. The monochromatic LCs in V and B (upper panel) are given by the thick and thin lines, respectively. The luminosity is shown in the lower panel.

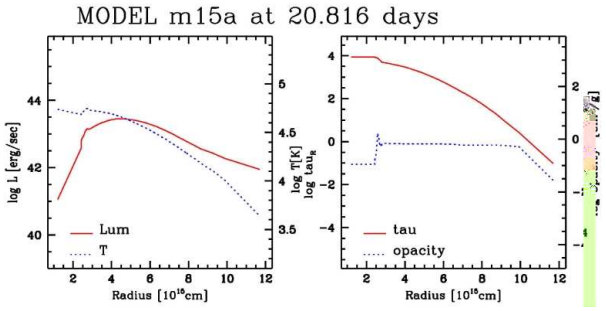

Figure 12. Luminosity, temperature, opacity and optical depth for the 15 $M_\odot$, Z=0.02 model (m15a) before the recombination phase, at day 20.

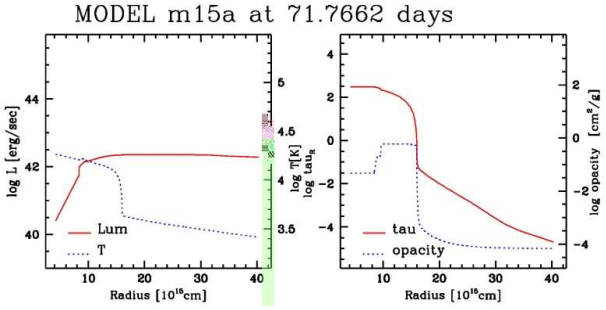

Figure 13. Same as Fig. 12 but during the recombination phase, at day 71.

long tail due to the energy release by radioactive decay of ^{56}Co (e.g. Fig. 11).

In the last 3 columns of Table 2 we show some properties of the light curves: the maximum visual magnitude (column 5), the length of the plateau phase, in days (column 6) and the size of the bump, in magnitudes, occurring at the end of the plateau phase (column 7). The length of the plateau is defined by the times when M_V becomes larger and smaller than $M_V(max) + 0.6^m$. In the table "dna" means do not apply.

Firstly, we consider the evolution of the structure for our reference model m15a, and the corresponding light curves (Figs. 11-13). The initial flash in the light curve is due to the energy deposition at shock breakout. Its duration is of the order of the sum of cooling time, the light crossing time of the stellar radius and the shock traveling time through the photosphere. For red supergiants, it is of the order of a few hours, for our blue supergiants about 10 minutes. For about 3 weeks after the explosion, the photospheric temperature is sufficient high to maintain ionization up to the outer layers (Fig. 12). The opacity is dominated by Thompson scattering, bound-free and free-free processes in the optical and IR, and by line blocking in the UV, resulting in very high optical depths of the envelope. Consequently, the expansion of the photosphere is strongly coupled to the expansion of the material. The diffusion time scales for photons, t_{diff}, are given by

$$t_{diff}(r) \approx \tau(r)^2 \cdot r/c$$

where τ is the optical depth, r the radius and c the speed of light. In our example at day 20, the diffusion time scales

exceed the expansion time scales in all layers up to about an optical depth of 10. As a consequence, the luminosity as a function of depth is not constant but it is increasing inward due to the stored energy released by the shock front and the receding (in mass) photosphere (Fig. 12). For the same reason, models with low explosion energies show a brightening between 30 to 50 days after the explosion.

After the initial rise, the reference model shows an *early plateau* not seen in observations. It is caused by the 1D nature of the model or, more precisely, due to the assumption that Ni is not mixed. For models with moderate explosion energies, the diffusion time scales for energy stored by radioactive decays is longer than the expansion time scale. As a consequence, the luminosity is solely provided by the thermal energy stored during the explosion because the contribution by radioactive decays is delayed. This effect is well known from models for SN1987A where mixing had to be assumed to avoid this artifact and to obtain good fits to the light curves observed (e.g. Woosley et al. 1988). Note that we do not see this early plateau in any observation. This may be a hint that the explosion mechanism is intrinsically aspherical and that mixing of the central layers is common in core collapse supernovae (see introduction).

With time, the photospheric temperature drops, and recombination of H sets in. Due to the strong drop in opacity with decreasing ionization, the position of the photosphere becomes almost stationary (Figs. 14). In Fig. 13, the structure of m15a is given at day 70 which is typical for the recombination phase. Diffusion time scales for the envelope become comparable to the expansion time scales. The luminosity is governed by the release of recombination energy which is deposited just below the photosphere. Typically, the ionization degree at the photosphere has dropped to 1 %. Therefore, the luminosity as a function of radius increases outward up to the photospheric radius and stays constant for the outer layers. The rate of the energy release depends on the recombination rate (in mass) and this depends on the mass flow through the photosphere, i.e. on the density slope n ($\rho \propto r^{-n}$). Since the density of the envelope is rather flat and slowly changing a self-regulating mechanism between energy release and heating of the photospheric region leads to an almost constant luminosity of the light curve. An increase in the energy release causes a heating of the photosphere and, thus, a higher degree of ionization and a larger opacity which, in term, reduces the luminosity and vice versa.

Eventually, the recombination front reaches the hydrogen-poor layers, and enters the He-core. At this point, the photosphere recedes very fast causing an energy release and a small bump in the light curve at the end of the recombination/plateau phase (see Fig. 11 and below). Thereafter, the energy is purely determined by the instantaneous energy input due to radioactive decays, mainly by ^{56}Co, up to a few hundred days after the explosion, then diffusion time scales become negligible. Except for models with extensive mixing of ^{56}Ni, the envelope above the radioactive elements remains optically thick for γ-rays and the high energy photons thermalize within the envelope almost completely.

At the onset of the recombination phase, B-V increases rapidly due to the drop in temperature and the increasingly strong line blocking. Subsequently, during the recombination phase, B-V changes slowly from about 1.2 to 1.5 magnitudes because the conditions remain similar at the photosphere. At the end of the recombination phase, again, B-V drops rapidly to about 2 magnitudes due to the strong line blocking in the B band, and due to a further decrease in temperature.

At the end of the plateau phase, the reference model shows brief period of increasing brightness in B and V, and bluer colors. This is caused by the rapid change in the He abundance at the photosphere which results in an increased recombination temperature and a more rapidly decreasing photosphere and, thus, a temporary increase in the release of stored energy. These effects should be strong in SNe with a low explosion energy. Both the late increase brightness and the decrease in B-V have yet to be observed. The lack of evidence for these effects may be regarded as further hint that, in reality, the inner layers of SNe are strongly mixed during the explosion.

The influence of the kinetic energy on the light curves is shown in Fig. 11. Overall, the shape of the light curve shows only some quantitative changes. Increasing the kinetic energy by a factor of 2 results on a faster rise of the light curve, an increased luminosity at the plateau ($\approx 0.27^m$ in the V band), and a slightly bluer color during the plateau phase. The overall similarities at the plateau are due to the similar density structures, as seen in the last section (see Fig. 9 and 10). The increase of E_{kin} results in a faster expansion rate of the material by about 40 %, and an increased energy deposition due to the shock front. Due to the faster geometrical dilution, the stored thermal energy is released faster, causing an increase in the early luminosity. During the early recombination phase, thermal energy still contributes to the flux. The increased mass flux through the photosphere increases the luminosity by about 30 to 40 % according to the increase in the expansion velocity. The higher flux results in a slightly bluer color of the more energetic model. In both models, we assume the same ^{56}Ni ejection and, consequently, the light curves become very similar after day 130 and the luminosity of the light curve tail are identical. However, the lower density requires a slightly higher color for the more energetic model to maintain the same integrated emissivity.

In Figure 15, we show the light curves for our set of models with Z=0.02 and different initial masses: 13, 15, 20 and 25 $M_\odot$, all of which explode as RSGs. The maximum brightness and the overall shape of the light curves remain very similar, showing a long plateau phase, in excess of 50 to 60 days and extending up to 80-130 days from the explosion time. We identify this group as an homogeneous subclass among Type II-P, i.e., *extreme* SN II-P. The mean brightness in V during the plateau ($\approx$ -17.4) is rather insensitive to the mass of the progenitor ($\Delta M_V \leqslant 0.07$ mag), and to the explosion energy if changed within a factor of 2. [1]. This suggest that this subclass, *extreme* SN II-P, may be used as quasi-standard candles with few free parameters, namely the Ni mass.

The similarity of the light curve shapes can be understood as a consequence of the similarity of the density slopes n (Fig. 10) that results in comparable energy production rates due to recombination. The main difference among the

[1] The explosion energy may be constrained by spectral observations

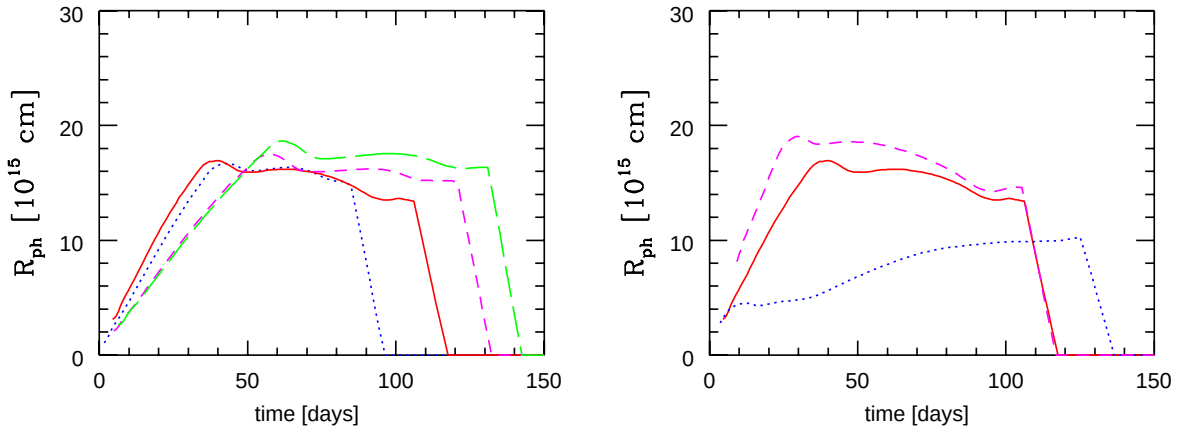

Figure 14. Photospheric radius as a function of time for models with the same metallicity, Z=0.02, but with different initial masses: 13 $M_\odot$ (dotted), 15 $M_\odot$ (solid), 20 $M_\odot$ (dashed) and 25 $M_\odot$ (long-dashed) on the left panel and for models with the same mass, 15 $M_\odot$, but different metallicities and/or kinetic energies on the right panel: Z=0.02 and 1 foe (solid), Z=0.02 and 2 foe (dashed) and Z=0 and 1 foe (dotted) on the right panel.

light curve is the length of the plateau phase because of the increase in the total hydrogen mass that is available as a reservoir for storing ionization energy (see Table 2).

Compared to Litvinova & Nadëzhin (1983, 1985), our RSG models show a similar correlation between the brightness during the mid plateau stage and the kinetic energy but a much weaker relation to the envelope mass. We have used the relations (4) and (5) from Litvinova & Nadëzhin (1985) to compute the mean V magnitude during the plateau and its duration in function of the explosion energy, R of the progenitor and the envelope mass. We obtain, for our mass range (envelope masses between 11.6 $M_\odot$ and 23.6 $M_\odot$) and in contrast with our models, that the mean V magnitude increases with mass; a variation of 0.23^m is obtained through the whole mass interval to be compared with the variation of 0.07^m resulting from our models. The duration of the plateau obtained using Litvinova & Nadëzhin equation increases with envelope mass as expected but, for all cases, is about 20 to 50 % times longer than the duration resulting from our models. These discrepancies can be understood as a consequence of the progenitor structure (see introduction). Litvinova & Nadëzhin (1983, 1985) use parameterized density structures with the stellar radius as a free parameter whereas our models are based on stellar evolution. In particular, Litvinova & Nadëzhin (1985) change the the envelope mass from 16 to 1 $M_\odot$ but assume the same radius. As a consequence, the column densities of the envelope differ by a factor of 16 and, consequently, the speed of the energy release. In contrast, our models m20a and m15a have an envelope mass of 18.6 and 13.6 $M_\odot$ but the radius decreases from 970 to 670 $R_\odot$ and the column densities in the envelope at a given radius are rather similar.

For a blue supergiant, i.e. m15z, the density slopes are much steeper compared to our reference model m15a (Fig. 10). Starting from a more compact envelope the cooling by adiabatic expansion increases, while the overall luminosity decreases by more than a magnitude. The maximum V magnitude at the plateau phase decreases by 1.3^m (Table 2). In this case the light curves do not show the long plateau phase (see Fig. 16) but a slowly rising up to the maximum light.

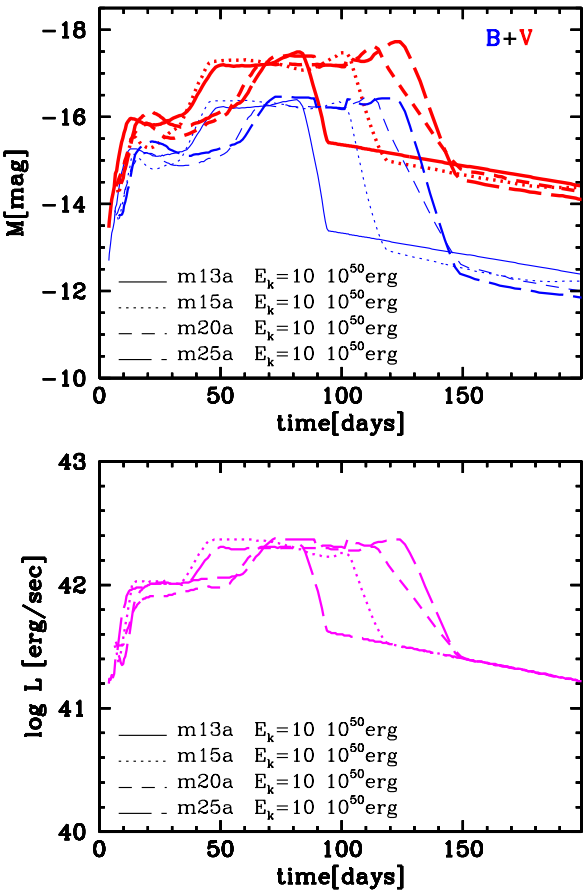

Figure 15. Light curves for models with the same composition (Z=0.02) and final kinetic energy (10^{51} erg) but different initial masses: 13 $M_\odot$ (m13a), 15 $M_\odot$ (m15a), 20 $M_\odot$ (m15a) and 25 $M_\odot$ (M25a). The monochromatic LCs in V and B are given by the thick and thin lines, respectively.

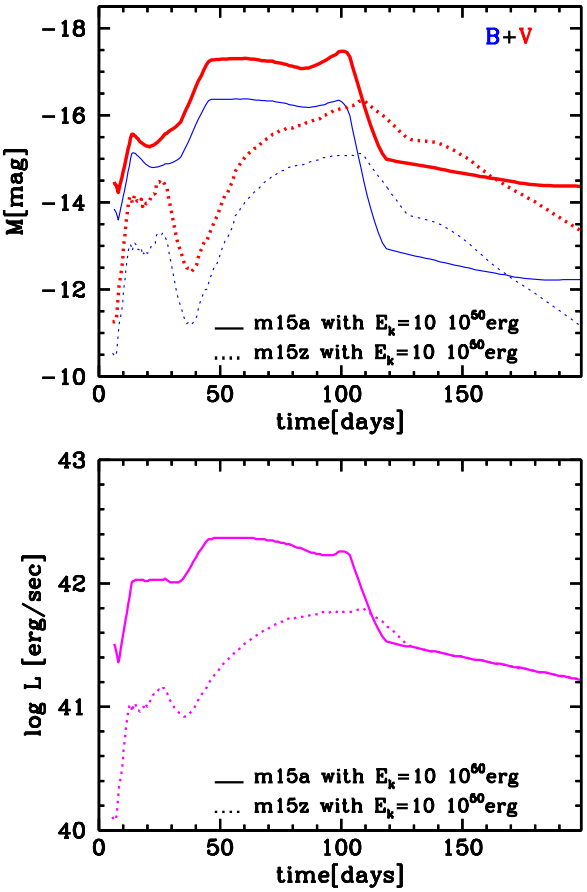

Figure 16. Light curves for models with the same mass, 15 $M_\odot$, and kinetic energy, 10^{51} erg, but different metallicities, Z=0.02 (m15a) and Z=0.0 (m15z). The monochromatic LCs in V and B are given by the thick and thin lines, respectively.

This is due to the steep density slope that causes a strongly increasing recombination rate as a function of time.

As a test to confirm this results, we have also computed the explosion and light curves for models with Z=0.0 and initial masses 20 and 25 $M_\odot$, as expected from the density gradients, the light curves show the same properties as m15z. Note also that line blocking in B and, in particular, in the UV, depends also on the metallicity, decreasing B-V for the low metallicity models.

4 CONCLUSIONS

We have studied theoretical B, V and bolometric light curves for type II plateau supernovae. Based on a set of stellar evolution calculations, we have analyzed the sensitivity of the light curves properties to the mass and metallicity of the progenitor and, within a factor of 2, to the explosion energy. We linked the pre-SN evolutionary models to SN models. Compared to previous studies, one big advantage is that the initial radius of the SN models is no longer an adjustable parameter but a result of the physical model and a function of the stellar mass, changing significantly the relation between progenitor mass and light curves. The other progress is that the hydro models are linked to a radiative transport code, so the broad-band light curves are much more accurately computed. A third progress provided by this study is the effect of metallicity in the resulting light curves.

We find the following main results within the parameter space considered:

For high metallicities, the stars explode as RSG regardless of the initial mass, showing a long plateau phase, longer than 50-60 days and extending up to 80-130 days after the explosion (*extreme* SNe II-P). They can be understood as explosions of Red Supergiants that have undergone rather moderate mass loss during the presupernova evolution. The V brightness during the plateau phase changes/declines by about 0.2 to 0.7^m. The mean absolute brightness in V ($\approx -17.5^m$) during the plateau phase is rather insensitive to the mass of the progenitor and the explosion energy (within $\approx 0.3^m$). Note that line blocking in B and, in particular, in the UV depends on the metallicity causing a somewhat larger spread.

The overall similarity of the LCs is caused by the similarity of the density structures of the red giant envelopes, and by the self-regulating propagation of the recombination front that determines the brightness during the plateau phase. For explosion energies less than 10^{51} erg, the self regulating mechanism between photospheric radius and the location of the recombination front will break down because the mean temperature of the envelope will drop below the recombination temperature. As a consequence, the absolute brightness during the plateau should drop fast with E_{kin}.

The metallicity plays a major role in determining the radius of the star because it affects the opacity that determines directly the super-adiabatic gradient that holds in the more external layers. The larger the opacity, the larger the super-adiabatic gradient and hence the larger the radius of the star. This explains why for low metallicities, stars explode as blue supergiants. The steep density profile results in a long lasting phase of increasing photospheric radius and brightness. The maximum brightness is lower by about 1.5^m compared to the explosion of a RSG because of the increased expansion work for BSGs. Qualitatively, this tendency is consistent with SN1987A. However as shown above, a 13 $M_\odot$ star will explode as a RSG even for Z as low as a 10^{-3}.

The mass dependence of the final outcome has two main consequences. Firstly, the discovery probability for SNe II at high z will decrease with the progenitor mass. The supernovae statistics will be systematically biased, starting at $z \approx 1$. The consequences for the study of the chemical evolution and the element production at high red-shifts (e.g. by NGST) shall be noted. Secondly, even at high redshifts, some *extreme* SNe II-P should be visible. Taking their unique properties, they may prove to be the key for the use of SN for cosmology at high z before SNe Ia occur. It is worth noting, that the photospheric temperatures at the shock breakout are higher than in the solar metallicity models. As the cross section for H-photoionization decreases with increasing frequency, $\sigma_\nu \propto \nu^{-3}$, the ionized circumstellar region around these SNe would be larger compared to the RSG case. The possible consequences for the re-ionization in the early universe may be noted.

Our results may be suggestive to the use of a subclass of SNe II, the *extreme* SNe II-P, as quasi standard candles. Although the use of *extreme* SNe II-P will not achieve the same accuracy as Type Ia Supernovae, there are some dis-

tinct advantages: 1) due to their unique light curves and colors, no spectrum is required for identification; 2) the requirements on the time coverage of the light curves are very moderate: three or four deep images with a sample rate of 50 to 60 days in the rest frame will allow their discovery, identification and their use for cosmology - at some time, two color images should be taken to deselect flare star and to get a handle on the reddening; 3) finally, there is no need to follow the light curves after the plateau toward dimmer magnitudes. For the use of SNe Ia, the requirement to obtain a spectrum limits their use to $\approx 24^m$ if 8m-class telescopes are employed. For the *extreme* SN II-P, 1) to 3) implies that the largest ground based telescopes with IR detectors can be used as search instruments which pushes the limit to about 27 to 28^m. Therefore, *extreme* SNe II-P may be used up to $z \approx 3$ using 8-meter class telescopes. SIRTIF may push the limit by another magnitude by long time exposures. Our results may be interesting with respect to the use of supernovae as distance indicators, and the supernovae statistics that may be constructed based on future observations by upcoming instruments such as NGST, SNAP and the like. For moderate to high metallicities, *extreme* SNe II-P may be used as standard candles with an accuracy of about 30% if, in addition, the color information is taken into account. Though not comparative with SNe Ia at low redshifts, their use may provide a valuable tool to supplement SNe Ia distances in our local universe.

At moderate redshifts (e.g. z=3-3.5), intergalactic metals have been discovered in the Lyα forest clouds showing metal abundance of 10^{-2} to 10^{-3} $Z_\odot$ (Songaila 1997, Cowie and Songaila 1998 and Ellison et al. 2000), so it will still be possible to find *extreme* SNe II-P as distance indicators.

We have also to stress the limits of our investigations which will require further studies. For our purposes, we have explored a limited range of parameters. Recent observations show a wide range of explosion energies and Ni masses well beyond the 'classical' estimates of 1 and 2 foe and 0.07 $M_\odot$ of Ni.

Hamuy (2002) found Ni masses between 0.0016 to 0.26 $M_\odot$, and kinetic energies from $0.6 \cdot 10^{51}$ to $5. \cdot 10^{51}$ for envelope masses between 14 to 56 $M_\odot$. Hamuy's interpretation for the kinetic energy and progenitor mass is based on extrapolation of the empirical relations by Litvinova & Nadëzhin (1983, 1985) which have been obtained for envelope masses between 1 and 16 $M_\odot$ and on parameterized structures (see also Section 3.3). Thus, the masses and explosion energies may be very uncertain. The importance of the progenitor structure becomes also evident in a direct comparison between estimated progenitor mass of SNe II-P based on LCs and non-detections of progenitors. Based on SNe observations and on hydrodynamical models (Litvinova and Nadëzhin, 1983, 1985), Hamuy obtained progenitor masses of 43(+24/-14) $M_\odot$ and 27(+14/-18) $M_\odot$ for SN1999gi and SN1999em, respectively. From the length of the plateau phase for SN1999em, Höflich et al. (2000) found models with $15M_\odot$ to be consistent with observations. Based on non-detection of the progenitor on archive images and stellar evolution, Smartt (2001,2002) found upper mass limits of 9(+3/-2) $M_\odot$ and 12±1 $M_\odot$ for SN1999gi and SN1999em, respectively. However, despite the problems, Hamuy's estimates of the total amount of ^{56}Ni are hardly effected by the model assumptions. A significant change in Ni will change the absolute brightness because radioactive decay contributes to the thermal reservoir feeding the light curves.

As discussed in section 3.3, mixing of the central layers will change the early rise and the late plateau phases. Such mixing must be expected from explosion models and should be included to improve the accuracy of the models.

No mass loss has been taken into account. Therefore, these models must be considered as extreme cases, limiting severely their use for the analysis of observations. In particular, strong mass loss of RSG will effect the relation between the envelope mass and the stellar radius differently from the change of the initial mass that determines the structure of the stellar core. Likely, this will increase the spread in parameter space. One further potential pitfall for SNe II is the anisotropic luminosity caused by aspherical explosions of core collapse SNe. In general, the light of core collapse supernovae is polarized by $\approx 0.5 \pm 1\%$ (e.g. Wang et al. 2001, Leonard et al. 2001, 2002). Polarization of this size corresponds to asymmetries in the envelope that produce directional dependence in the observed L of ≈ 0.3 *to* 0.6^m (Höflich, 1991). However, extended H rich envelopes tend to spherize the H-rich layers of the envelopes even if the explosions are assumed jet-like (Höflich, Khokhlov & Wang, 2001). This tendency is consistent with recent observations for SN1999em.

In summary, the typical light curves and colors of our *extreme* SN II-P models are, at first order, in agreement with observations but a quantitative comparison and statistical analyzes with observations must be postponed till complete data sets become available, and the model grid has been extended. If done, such comparison may be used to get an insight of details of the physics, like fallback during the explosion, realistic predictions for the nucleosynthesis and constrains for core collapse models. For the application to cosmology and to get a handle on the interstellar reddening, the color information must be considered and spectral information may be used to increase the accuracy. Taking current initiatives, e.g. CSP (Carnegie Supernova Program), LOTOSS (Lick Observatory and Tenagra Observatory Supernova Searches), NEAT (Near-Earth Asteroid Tracking), SDSS (Sloan Digital Sky Survey) and the upcoming SNAP and NGST missions, we expect an increasing availability of high quality data.

ACKNOWLEDGMENTS

PAH would like to thank the people at the Observatories in Teramo and Monteporzio (Italy) for the hospitality during his stay when this paper was born. ID thanks the people at the Dept. of Astronomy (University of Texas) at Austin for their hospitality during her stay when this paper was finished and thanks Mario Hamuy for his careful reading of the manuscript. This research was supported in part by NASA Grant LSTA-98-022, by the Italian grant MURST-Cofin2000, by the Spanish grant AYA2000-1574, AYA2002-04094-C3-03 and by the Andalusian grant FQM-292. The calculations for the explosion and light curves were done on a cluster of workstations financed by the John W. Cox-Fund of the Department of Astronomy at the University of Texas.

REFERENCES

Alexander, D.R., and Fergusson, J.W. 1994, ApJ, 437, 879
Arnett W.D., Bahcall J.N., Kirshner, R.P., Woosley, S.E. 1990, ARAA 27, 62
Beaudet, G., Petrosian, V., and Salpeter, E.E. 1967, ApJ, 150, 979
Bisnovatyi-Kogan 1971, Soviet Astronomy AJ, 14, 652
Bowers R.L., Wilson J.R. 1982 ApJS 50, 115
Branch D. 1988, Proc. of the Symp. on Extragalactic Distance Scales, ed. van den Bergh, Springer Press
Brunish W.M., Truran J.W 1982, ApJ 49, 447
Burrows A., Hayes J., Fryxell B.A. 1995 ApJ 432, 830
Cappellaro E., Evans, R., Turatto, M. 1999 A&A 351, 459
Castellani, V., Chieffi, A, Pulone, L., and Tornambè, A. 1985, ApJ, 296, 204
Caughlan, G.R., Fowler, W.A., Harris, M., and Zimmerman, B. 1985, At. Data Nucl. Data Tables, 32, 197
Chieffi, A., and Straniero, O. 1989, ApJs, 71, 48
Chieffi, A., Limongi, M., and Straniero, O. 1998, ApJ, 502, 737
Chieffi, A., and Limongi, M. 2002, ApJ, 577, 281
Colella, P, Woodward, P.R. 1984, JCoPh 54, 174
Cowie, L.L., and Songaila, A. 1998, Nature, 394, 248
Cox, J.P., and Giuli, R.T. 1968, in Principles of Stellar Evolution, Vol. 1, (New York:Gordon and Breach), 281
De Witt, H., Graboske, H., and Cooper, M. 1973, ApJ, 181, 439
Dicus, D.A., Kolb, E.D., Schramm, D.N., and Tubbs, D.L. 1976, ApJ, 210, 481
Eastman R.G., Woosley S.E., Weaver T.A., Pinto P. 1994, ApJ 430, 300
Ellison, S.L, Songaila, A., Schaye, J., and Pettini, M. 200, AJ, 120, 1167
Fesen, R. A. & Gunderson, K. S. 1997, ApJ, 470, 967
Filippenko A.V. 2000 in *Cosmic Explosions*, Eds. S. Holt & W.W. Zhang, New York: American Institute of Physics
Fuller, G.M., Fowler, W.A., and Newman, M. 1980, ApJS, 42, 447
Fuller, G.M., Fowler, W.A., and Newman, M. 1982, ApJs, 48, 279
Fuller, G.M., Fowler, W.A., and Newman, M. 1985, ApJ, 293, 1
Garnavich et al. 1998a ApJ, 509, 74
Garnavich et al. 1998b ApJ, 493L, 53
Graboske, H., De Witt, H., Grossman, A., and Cooper, M. 1973, ApJ, 181, 457
Grevesse, N. 1991 in Evolution of Stars: The Photospheric Abundance Connection, ed. G. Michaud and A. Tutukov, (Dorddrecht: Kluwer), pg. 63
Hamuy, M., and Pinto, P.A., 2002, ApJ 566, L63
Hamuy, M., 2002, ApJ , in press (astro-ph/0209174)
Hamuy, M. et al. 1996, AJ, 112, 2391
Heger, A., Langer, N., Wppsley, S.E. 2000, ApJ 528, 368
Herant M., Benz W., Hix W.R., Fryer C.L., Colgate S.A. 1994, ApJ 435, 339
Hillebrandt W. 1982, ApJ 103, 147
Hillebrandt W., Höflich 1991, Nuclear Physics B, 19, 113
Höflich P., Wehrse R., Shaviv G. 1986, A&A 163, 105
Höflich P. 1988, PASAu 7, 434
Höflich P. 1991a, in "Supernovae",, ed. S.E. Woosley, Springer Press, New York, p. 415
Höflich P. 1991b, A&A 246, 481
Höflich, P. 1995, ApJ 443, 89
Höflich P., Khokhlov A. 1996, ApJ 457, 500
Höflich P., Wheeler J.C., Thielemann F.K 1998, ApJ 495, 617
Höflich P., Straniero O., Limongi M., Domínguez I., Chieffi A. 2000, 7th TexMex- Conference, eds. W. Lee & S. Torres-Peimbert, UNAM-Publ., p. 157 & astro-ph/0005037
Höflich P., Khokhlov A., Wang L. 2001, 20^{th} Texas Conference on Relativistic Astrophysics, eds. H. Martel & C. Wheeler, AIP Conference Proceedings 586, p. 459 & astro-ph/0104025
Höflich P., Khokhlov, Wang, L., Wheeler J.C., Baade, D. 2002 in A Massive Star Odyssey: from Main Sequence to Supernova, IAU Symposium N. 212, Ed. K.A. van der Hucht, A. Herrero & C. Esteban, astro-ph 0207272
Hoyle P., Fowler W.A. 1960, ApJ 132, 565
Huebner, W.F., Merts, A.L., Magee, N.H., and Argo, M.F. 1977, Los Alamos Sci. Lab. Rept. (LA-6760-M) (LAOL)
Huges J.P., Rakowski C.E., Burrows D.N., Slane P.O. 2000, AJ, submitted & astro-ph/9910474
Iben I.J, Tutukov A.V. 1984, ApJS 54, 335
Iglesias, C.A., Rogers, F.J., and Wilson, B.G. 1992, ApJ, 397, 717 (OPAL)
Itoh, N., Totsuji, H., and Ichimaru, S. 1977, ApJ, 218, 477
Itoh, N., Totsuji, H., Ichimaru, S., and De Witt, H. 1979, ApJ, 234, 1079
Itoh, N., Mitake, S., Iyetomi, H., and Ichimaru, S. 1983, ApJ, 273, 774
Janka H.T., Müller E. 1996, A&A 306, 167
effrey D.J., 1991, ApJ, 375, 264
Khokhlov A., Höflich P., Oran, E.S., Wheeler, C.J., Wang, L., ChtChelkanova, A.Y. 1999, ApJ 524, 107
Kravtso A.V., Yepes G. 2000, MNRAS 318, 227
Kurucz, R.L. 1991, in Stellar Atmospheres: Beyond Classical Model, ed. L. Crivellari, I. Hubeny, and D.G. Hummer (Dordrecht:Kluwer), 441
LeBlanc, J. M. & Wilson, J. R. 1970, ApJ, 161, 541
Leonard, D.C., Filippenko, A.V., Chornock, R., Foley, R.J. 2002, PASP 114, L1333
Leonard, D.C., Filippenko, A.V., Ardila, D.R., Brotherton, M.S. 2002, ApJ 553, L861
Limongi M., Chieffi A., Straniero O. 2001 ApJS 129, 625L
Limongi, M., Straniero, O., Chieffi, A. 2000, ApJS 129, 625
Litvinova, I.Y., and Nadhëzin, D.K. 1985 SvA, 11, 145
Litvinova, I.Y., and Nadhëzin, D.K. 1983 Ap&SS., 89, 89
Marri S., Ferrara A. 1998, ApJ 509, 43
Marri S., Ferrara A., Pozzetti L. 2000, MNRAS 317, 265
Maza J., van den Bergh, S. 1976, ApJ 204, 519
Méndez M., Clocchiatti A., Benvenuto G., Feinstein C., Marraco U.G., 1988, ApJ, 334. 295
Miralda-Escudé, J., Rees, M.J. 1997, ApJ 478, 57
Meynet, G., Maeder, A. 2000, A&A 361, 101
Meynet, G., Maeder, A. 2003, A&A accepted (astro-ph/0304069)
Mönchmeyer R., Schaefer G., Mueller E., Kates R.E. 1991 A&A 246, 417
Müller, E., and Höflich, P. 1991 in ESO Workshop on Supernovae. Eds. J. Danzinger et al., ESO publishing, p. 379
Müller E., and Höflich P. 1984, ApJ 484L, 57
Müller E., Janka H.T. 1997, A&A 317, 140

Munakata, H., Kohyama, Y., and Itoh, N. 1985, ApJ, 296, 197
Munakata, H., Kohyama, Y., and Itoh, N. 1986, ApJ, 304, 580
Nugent P., et al. 1996, Phys.Rev.Let. 75, 394 & 1974
Paczyński B. 1985, in *Cataclysmic Variables and Low-Mass X-Ray Binaries*, eds. D.Q. Lamb & J. Patterson, (Dordrecht: Reidel) p. 1
Patat F., Barbon R., Capellaro E., Turatto M. 1993, A&Aps 98, 443
Patat F., Barbon R., Capellaro E., Turatto M. 1994, A&Ap 282, 731
Perlmutter, S., et al. 1999, ApJ 517, 565
Phillips M.M. et al. 1987, PASP, 90, 592
Phillips M.M., Lira P., Suntzeff N.B., Schommer R.A., Hamuy M., Maza J. 1999, AJ 118, 1766
Richardson, M.B., Van Horne, H.M., Ratcliff, K.F., and Malone, R.C. 1982, ApJ, 255, 624
Riess A.G., Press W.H., Kirshner R.P. 1996, ApJ, 473, 588
Riess A.G., et al. The High-z Team, 1998, AJ 116, 1009
Riess A.G., et al. The High-z Team, 2001, ApJ 560, 49
Saenz R.A., Shapiro S.L. 1981, ApJ 244, 1033
Saha P. Sandage A., Labhardt L., Tammann G., Macchetto F.D., Panagia N. 1997, ApJ 486, 1
Schmidt B.P., Kirshner R.P., Eastman R., Hamuy M., Phillips M.M., Suntzeff N.B., Maza J. Filippenko A.V., Ho L.C., Matheson T., Grashuis R., Aviles R., Kirkpatrick J.D., Challis P., Kuijken K., Zucker D., Bolte M., Tyson N.D. 1994, AJ 107, 1444
Schmidt B.P. et al. 1998, ApJ 507, 46
Shaviv G., Wehrse R., Wagoner R. 1985, ApJ 298, 189
Smartt, S.J., Gilmore, G.F., Trentham, N., Tout, C., Frain, C.M. 2001, ApJ 556L, 29
Smartt, S.J., Gilmore, G.F., Hodgkin, S.T. 2002, ApJ 565, 1089
Songaila, A. 1997, ApJ 490, L1
Sparks, W.M., and Endal, A.S. 1980, ApJ, 237, 130
Straniero, O. 1988, A&Aps, 76, 157
Straniero, O., Chieffi, A., and Limongi, M. 1997, ApJ, 490, 425
Strom R., Johnston H.M., Verbunt F., Aschenbach B. 1995, Nature, 373, 587
Tammann G., 1982 in NATO-ASI on Supernovae: A Survey of Current Research, Eds. M.J. Rees and R.J. Stoneham, Reidel, Dordrecht, p. 371
Tueller J., Barthelmy S., Gehrels N., Leventhal M., MacCallum C.J., Teegarden B.J. 1991, in: Supernovae, ed. S.E. Woosley, Springer Press, p. 278
Van Riper K.A. 1978, ApJ 221, 304
Wang, L., Wheeler, C.J., Höflich, P., 1997, ApJ 476, L27
Wang, L., Howell, A., Höflich, P., and Wheeler, J.C., 2001, ApJ 550, 1030
Wang L., Wheeler C.J., Höflich P., Khokhlov A., Baade D. + SINS-team, 2002. ApJ, accepted & astro-ph0205337
Wang, L., Wheeler, J. C., Li, Z. W., & Clocchiatti, A. 1996, ApJ, 467, 435
Wang, L., Wheeler, J. C. & Höflich, P. 1999, in SN 1987A: Ten Years After, ed. M. M. Phillips and N. Suntzeff (Provo: Ast. Soc. of the Pacific), in press
Wang, L., Wheeler, J. C., Li, Z. W., & Clocchiatti, A. 1996, ApJ, 467, 435
Webbink R.F. 1984, ApJ, 277,355
Whelan J., Iben I.Jr. 1973, ApJ 186, 1007
Woosley S.E., Weaver T.A. 1986, ARA&A 24, 205
Woosley S.E., Pinto P.A., Weaver T.A. 1988, PASAu 7, 355
Young T.R., Branch D. 1989, ApJ 342, L79